First principle-based simulation of ethane steam cracking

ARTICLE *in* AICHE JOURNAL · FEBRUARY 2011

Impact Factor: 2.75 · DOI: 10.1002/aic.12269

AIChE

First Principle-Based Simulation of Ethane Steam Cracking

Maarten K. Sabbe, Kevin M. Van Geem, Marie-Françoise Reyniers, and Guy B. Marin
Laboratorium voor Chemische Technologie, Universiteit Gent, Krijgslaan 281 S5, B-9000 Gent, Belgium

DOI 10.1002/aic.12269
Published online April 28, 2010 in Wiley Online Library (wileyonlinelibrary.com).

A consistent set of ab initio-based kinetic and thermodynamic data is applied for the simulation of an ethane steam cracking furnace. The thermodynamic data are calculated using accurate quantum chemical CBS-QB3 calculations including corrections for hindered internal rotation. The kinetics are obtained from CBS-QB3-based group additive models. With these thermodynamic and kinetic data, simulations for pilot and industrial ethane steam cracking reactors over a wide range of process conditions are performed. It is shown that, without adjusting any parameter, the main product yields can be predicted within 15% rel. of the experimentally observed cracking yields. This indicates the tremendous potential of integrating ab initio methods with engineering models for accurate reactor simulations. © 2010 American Institute of Chemical Engineers
AIChE J, 57: 482–496, 2011
Keywords: ab initio, group additivity, radical chemistry, reactor simulation, steam cracking

Introduction

Kinetic modeling plays a pivotal role in the design and optimization of chemical process plants. The capability to predict reliably the behavior of chemical reactions over a broad range of temperatures and pressures would, in principle, enable the a priori design of new chemical reactors and chemical processes. In recent years, it has become possible to predict accurately the behavior of some rather complex gas phase chemical reaction mechanisms such as, for instance, the atmospheric chemistry involved in ozone depletion[1–4] or the chemistry occurring in steam cracking and pyrolysis of hydrocarbons.[5–7] The development of these models required a tremendous experimental effort, spread over several decades, involving a huge amount of work by many researchers. More efficient methods for the development of kinetic models are absolutely required. These methods should be able to reliably predict the chemistry involved in chemical processes so that they can be used as a predictive tool for process design and optimization.[8] However, for an a priori prediction of the behavior of even well-established gas phase industrial processes, several technical hurdles need to be overcome. This work aims to provide proof-of-principle that the complex kinetic behavior in radical gas phase reaction mechanisms can be reliably predicted over a broad range of conditions by integrating quantum chemistry techniques with engineering models at larger length and time scales, that is, to show that ab initio modeling of gas phase reactions from molecular to industrial scale has now come within reach.

A reactor simulation, the common tool for reactor optimization, is based on a combined description of the physical and chemical phenomena that occur in the chemical reactor. The intrinsic chemical reaction rates are described using a kinetic model that is combined with a reactor model that accounts for the conservation laws and incorporates the physical transport phenomena. The development of reactor models is rather advanced and well established, particularly for the most commonly used chemical reactors in industry. Because of limitations in analytical chemistry, computer hardware and software capabilities, most traditional process

Additional Supporting Information may be found in the online version of this article.

Correspondence concerning this article should be addressed to M.-F. Reyniers at mariefrancoise.reyniers@ugent.be.

models, however, implement lumped kinetics schemes, in which the molecules are grouped by global properties such as boiling point or solubility. Even in recent years, apart from some exceptions,[9] more complex kinetic models are scarcely used in the industry.[10] The globally lumped and nearly ''chemistry-free'' kinetic models are specific in nature and can, for example, not be extended to new feedstocks. However, stricter environmental regulations, such as the Clean Air Act and the Kyoto protocol, and tighter technical requirements, such as the need to improve the product quality and performance, have lead to the new paradigm to track each molecule in both the feed and product throughout the process stream. Molecule-based models can incorporate information from quantum chemical level to full process scale and can hence serve as a common fundamental tool for both process development and chemistry research. Therefore, the future in kinetic modeling will be in detailed kinetic models, consisting of elementary reactions.

For radical chemistry, on which many of the world largest scale chemical processes are based, the reactive nature of the radical intermediates results in a complex chemistry, that is, in huge reaction networks typically involving hundreds of species and several thousands of elementary reactions.[11] Because of the large number of elementary reactions involved, reaction network generation evolved from manual construction[12,13] to computer-aided generation using advanced algorithms for the selection of the relevant reactions.[7,8,14–20] These algorithms generate a reaction network starting from the feedstock molecules and a given set of reaction rules, yielding all possible intermediates and reactions.

Providing these detailed reaction networks with accurate values for the required thermodynamics and kinetics in the desired range of conditions is one of the largest challenges in the modeling of industrial processes based on radical chemistry. As experimental determination of rate coefficients is very time consuming and, in particular for radical reactions, very complicated, experimental kinetic data are by far too scarce to describe the necessary kinetics. Generally, a combination of experimentally determined, predicted, and fitted data is applied to overcome the lack of available kinetic and thermochemical data.[5–7,21] Quantum chemistry provides an opportunity to provide these reaction schemes with consistent data, thanks to the advances in methods in computing power last decennia. The use of quantum chemistry to calculate rate coefficients for gas phase radical reactions is particularly attractive since it avoids difficult experimentation techniques and the need to rely on assumed reaction schemes. However, calculating accurate kinetics and thermodynamics for the thousands of reactions for radical chemistry is beyond computational possibilities. Therefore, engineering approximations are introduced that have the advantage that for the larger species and reactions in the network, for which accurate quantum chemical calculations are computationally too expensive, the thermodynamics and kinetics can be reliably determined based on ab initio calculations involving only smaller species. Recently, several parameterization schemes for rate prediction have been constructed based on ab initio calculations.[22–29]

In previous work, consistent group additive models have been constructed for the prediction of thermochemistry and kinetics for the radical gas phase chemistry of hydrocarbons.[28–32] These models are based on the ab initio calculation of a consistent set of thermodynamic and kinetic data for the most important reaction families involved in radical hydrocarbon chemistry. The methodology is based on Benson group additivity and has proven its reliability for hydrocarbon thermochemistry[30,31] and the kinetics of radical additions and hydrogen abstractions.[27–29,33] The ab initio computational method, CBS-QB3,[34,35] has already shown its accuracy for hydrocarbon gas phase chemistry.[30,31,36–40]

A successful simulation of an industrial reactor can provide proof-of-principle that the current computational quantum chemical methods can be integrated with engineering models at larger length and time scales and, hence, that reliable ab initio modeling of gas phase reactions from molecular to industrial scale has come within reach. Steam cracking of ethane was chosen as a test case for several reasons. First, it is a well-established process and the detailed radical chemistry is fairly well known. Second, kinetic models for steam cracking typically describe the data adequately, without the need to include pressure dependent kinetics,[7,11,14,41–44] that is, reactor simulations can be performed with a single set of fixed-pressure rate coefficients. Therefore, pressure dependence is not a key factor in steam cracking modeling and high pressure ab initio results can be expected to give fairly reliable results without additional effort to account for pressure dependence. Third, an extensive experimental database covering a broad range of conditions is available in our group, allowing to compare the simulation results with experimental data obtained on a pilot plant scale. In addition, in-house developed, microkinetic (CRACKSIM)[7,14,42,43,45] and reactor modeling tools (COILSIM)[45] for steam cracking are also available in our group. The detailed reaction network and rate coefficients used in CRACKSIM are based on an extensive experimental database and provide a very reliable simulation of industrial ethane and naphtha steam crackers.[44,45] A comparison of the ab initio-based simulation results with industrial data and with simulations using COILSIM thus provides the ultimate test of the validity of the group additive schemes and of the methodology developed in this work. Moreover, in the current reaction networks for the simulation of steam cracking reactions, such as CRACKSIM[45] or SPYRO,[6,46,47] the applied kinetic and thermodynamic data are typically a mixture of experimental, predicted, and fitted data. Particularly, because of the fitting of kinetic data to experimental results, it is not guaranteed that the reaction network accurately describes all the kinetically relevant underlying chemistry since deficiencies in the network might be compensated by a bias on the rate coefficients of other reactions. In that respect, performing a full ab initio-based simulation can help to establish the intrinsic validity of the reaction network, which is an additional advantage of the approach used in this work.

Methodology

Reaction network and reactor modeling

Nowadays, computers are used not only to solve the reaction model equations numerically but also to generate the network, construct the model, and calculate the kinetic parameters. Because such microkinetic models may contain up to thousands of reactions and species, constructing them by

hand can be tedious and error-prone. Therefore, many research groups have developed computer tools to automatically generate these reaction networks.[7,14,16,48–56] A key difficulty of these network generation programs is that they produce large numbers of kinetically unimportant reactions and species. Therefore, sometimes expert user involvement is used to limit the size of the reaction network. Several assumptions are commonly made when generating reaction networks for steam cracking and pyrolysis, to limit the network size and network generation time.[11,13,14,19] Although some of them can be supported by experimental evidence, for example, the μ-radical hypothesis for long-chain hydrocarbons,[11,13,19] still some doubts remain about others, for example, lumping of intermediate species or the quasi-steady-state approximation for certain species. To check the reliability of the ab initio data, the extensive reaction network for steam cracking, consisting of 1772 reversible reactions between 175 species generated using a carbon stop criterion as described by Van Geem et al.,[45] is compared with a rate-based generated network using only the ab initio thermodynamic and kinetic data for network generation.

Generally, a detailed reaction network is generated by allowing the feedstock components to react according to different reaction families. Examples are hydrogen abstraction reactions either intramolecular and intermolecular, addition reactions (intramolecular and intermolecular), etc. Rice and coworkers[12,57–59] showed that steam cracking of hydrocarbons proceeds through a free radical mechanism and that three important reaction families can be distinguished.

- Carbon–carbon and carbon–hydrogen bond scissions of molecules and the reverse radical–radical recombinations:

$$R_1 - R_2 \rightleftarrows R_1^\bullet + R_2^\bullet$$

- Hydrogen abstraction reactions, both intramolecular and intermolecular:

$$R_1 - H + R_2^\bullet \rightleftarrows R_1^\bullet + R_2 - H$$

- Radical addition to olefins and the reverse β scission of radicals, both intramolecular and intermolecular:

$$R_1^\bullet + R_2 = R_3 \rightleftarrows R_1 - R_2 - R_3^\bullet$$

Figure 1 shows how the reaction network is automatically generated. Starting from an initial pool of molecules, possibilities for scission reactions, hydrogen abstraction reactions, and addition reactions are identified. Cyclization reactions are considered as intramolecular additions, while isomerization reactions are considered as intramolecular hydrogen abstractions. For every forward reaction introduced in the network, the corresponding reverse reaction is also incorporated in the network. These reactions result in a number of formed radicals and molecules. The new radicals are added to the radical pool and the molecules are added to the molecule pool. In the next iteration, the new species react with each other and with other species of the radical and molecule pool and the network is constructed gradually.

A problem of this type of approach is that in principle the reaction network can become infinite, because addition reactions continuously lead to the formation of new species not yet included in the reaction network. Similar to Broadbelt et al.,[50] this problem has been overcome by using a carbon count stop criterion for the formed species to limit the network growth. Because no products with nine or more carbon atoms are identified in the ethane cracking experiments, the maximum carbon number species is set to eight. To further limit the size of the reaction network, the $\beta\mu$ rules of Goldfinger-Letort-Niclause[60] are applied. In steam cracking, acyclic radicals with more than five carbon atoms are considered μ radicals,[7,13] that is, they only react via monomolecular reactions. Small radicals, such as the ethyl or propyl radical, are usually allowed to react by both unimolecular and bimolecular pathways, that is, $\beta\mu$ radicals. Benzyl and methyl radicals on the other hand are usually assumed to react only bimolecularly (β radicals), that is, their unimolecular reactions are neglected. A computer program is developed that generates the reaction network automatically based on the binary relation matrix concept.[7] In this concept, the cracking rules are translated into matrix operations performed on the Boolean relation matrix, representing the species structure.[14] The calculation of the rate coefficients is discussed in the following paragraph.

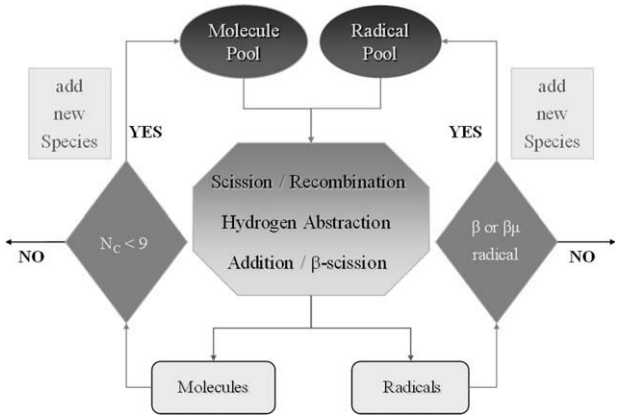

Figure 1. Automatic network generation using a carbon count stop criterion ($N_C < 9$) and $\beta\mu$ rules of Goldfinger-Letort-Niclause.[60]

In the pilot plant reactor, radial temperature, pressure, and concentration gradients are limited, allowing the use of one-dimensional reactor model equations.[44] The reaction equations are integrated using the in-house developed program COILSIM1D, which uses the implicit numerical software DASSL[61] to solve the stiff set of differential equations.[45] The process gas temperature and pressure profile in the simulations are taken from the corresponding pilot plant experiment. COILSIM1D is combined with the extensive reaction network.[45]

The steam cracking of ethane in an industrial cracker is simulated using a two-dimensional reactor model implemented in COILSIM2D.[44] The latter is necessary because important radial gradients exist in these type of reactors, not only for the temperature but also for the molecular and in particular the radical species.[44] The applied reactor equations and boundary conditions can be found in Van Geem et al.[44]

Table 1. Mean Absolute Deviations on Differences Between Calculated and Experimental Values

	$\Delta_f H°$(298 K) (kJ/mol)	$S°$(298 K) (J/mol/K)	Cp°(298 K) (J/mol/K)
Number of species	51	39	46
MAD	1.3	1.2	1.8

Thermodynamic and kinetic data

For all reactions in the reaction network, the kinetics and thermodynamics need to be known. Most network generation tools obtain the necessary thermochemical data from an electronic database of literature values, whenever possible. In most instances, however, the latter are not available and one must resort to group contribution methods to estimate standard enthalpies of formation, entropies, and heat capacities. In this case, a database of ab initio calculated thermodynamic data for 265 species is used, determined using the high-accuracy CBS-QB3 compound method with corrections for all internal rotations. The applied methodology yields very good agreement with experimental data for standard enthalpies of formation, entropies, and heat capacities (see Table 1).[30,31] As for the limited number of species for the cracking of ethane in this work all thermochemistry values were known ab initio, the ab initio obtained values are used directly for the determination of radical reaction thermodynamics, that is, without using group additivity.

Rate coefficients for the elementary steps have been determined using the group additive values obtained in previous work.[28,29,32] The model is based on the group additive model for calculation of activation energies introduced by Saeys et al.,[27] extended for pre-exponential factors including corrections for hindered rotation and tunneling. The activation energy and the pre-exponential factor are related to the structure of the transition state. For any reaction in the considered family, the pre-exponential factor and the activation energy are obtained by adding contributions to the reference values, which account for the structural differences between the considered reaction and the reference reaction. The pre-exponential factor obtained from the group additive method is finally multiplied by the number of single events, that is, the number of energetically equivalent reaction paths from reactant(s) to the transition state. The reference value of the pre-exponential factor is thus defined for the ''single event''. Considering single events and tracing structural analogies between the reaction gives a substantial reduction of the number of parameters in the model. The reaction rate coefficients are calculated according to:

$$k = \kappa n_e \tilde{k} = \kappa n_e \tilde{A} \exp\left(-\frac{E_a}{RT}\right) \quad (1)$$

$$E_a(T) = E_{a,ref}(T) + \sum_{i=1}^{n} \Delta GAV^{o}_{E_a}(C_i) \quad (2)$$

$$\log A(T) = \log \tilde{A}_{ref}(T) + \sum_{i=1}^{n} \Delta GAV^{o}_{\log \tilde{A}}(C_i) + \log n_e \quad (3)$$

in which $E_{a,ref}$ and $\tilde{A}_{ref}$ are the Arrhenius parameters of the reference reaction, the $\Delta GAV°$ are the group additive values, and n_e is the number of single events:

$$n_e = \frac{n_{opt,\ddagger}}{\prod_j n_{opt,j}} \frac{\prod_j \sigma_j}{\sigma_\ddagger} \quad (4)$$

with n_{opt} the number of optical isomers, σ the global symmetry number, and j running over the number of reactants. The use of group additive values relative to a reference reaction to calculate the activation energy and the pre-exponential factor of radical reactions results from the strong analogy that exists between the different reactions, considering their mechanism.[12]

On the basis of thermodynamic consistency, the reverse rate coefficients are calculated based on the forward rate coefficients and the thermodynamic equilibrium coefficient. The calculation of the standard Gibbs energy of reaction requires the knowledge of the thermodynamic properties, which are obtained from ab initio calculations as stated previously.

The group additive values are determined from a database of kinetic parameters calculated in the high pressure limit using the CBS-QB3 compound method taking into account the internal rotation about the forming/breaking bond. Rate coefficients are obtained using the conventional transition state theory with corrections for tunneling when necessary:

$$k_\infty(T) = \kappa(T) \frac{k_B T}{h} \frac{n_{opt,\ddagger} q_\ddagger}{n_{opt,A} q_A n_{opt,B} q_B} e^{-\frac{\Delta E(0K)}{RT}} \quad (5)$$

From several ab initio methods, this method was found to give the best agreement in comparison with experimental rate coefficients for a test set of 48 reactions spanning all the reaction families relevant to steam cracking. The CBS-QB3 method with hindered rotation and tunneling corrections yielded the lowest mean factor of deviation from the experimental values (see Table 2).[29,38,39]

At steam cracking conditions, the mean factor of deviation is a factor 3 on the rate coefficients. For hydrogen

Table 2. Mean Factors of Deviation <ρ> Between Calculated and Experimental Rate Coefficients

	Carbon Radical[38]		Hydrogen Radical[29]		Hydrogen[39]	
T (K)	Addition	β Scission	Addition	β Scission	Abstraction	Mean
300	2.1	3.3	1.7	2.3	10.0	3.9
600	3.2	2.5	1.5	2.2	3.9	2.7
1000	3.9	2.6	2.0	1.8	3.6	2.8
No. of reactions in test set	8	6	7	6	21	48

CBS-QB3 calculated rate coefficients with correction for internal rotation about the forming/breaking bond, and inclusion of tunneling correction for hydrogen addition and abstraction.

abstractions, the deviations are evenly distributed around the experimental values. For carbon and hydrogen radical additions, the calculated rate coefficients rather over than underpredict the experimental rate coefficients. This tendency might influence the accuracy of the calculated product yields in the reactor simulations.

Group additive models have been constructed for the reaction family of carbon-centered radical additions,[28] hydrogen radical additions,[29] hydrogen abstractions by carbon-centered radicals,[32] and by hydrogen radicals. In this work, the reported group additive values and the reference reaction Arrhenius parameters at 1000 K are applied. Many of the important reactions, particularly those involving methyl and hydrogen radicals such as the C-H β scission of the ethyl radical, have been used in the training set for the group additive values. Therefore, the group additive prediction for these reactions equals the ab initio rate coefficients.

For ring formation through intramolecular radical additions, reactions involved in benzene, and cyclopentadiene formation, direct ab initio kinetics were applied because group additive models are not available for these reaction families. Similarly, direct ab initio values were used for intramolecular hydrogen abstractions, which correspond to radical isomerization reactions.

The calculation of rate coefficients for C—C and C—H bond scission and radical recombination requires a different approach than for the other reaction families. Because radical recombination reactions are barrierless, there is no clear transition state present on the potential energy surface. Hence, canonical transition state theory does not yield reliable results. A variational transition state theory approach (VTST), in which the dividing surface between reactant and product valley is optimized for the minimum rate, needs to be used. However, due to the flatness of the potential energy surface, this dividing surface is strongly influenced by the energy and the angular momentum of the collision. Moreover, the nature of the interactions changes from long-range to covalent, while the large-amplitude interfragment motions are complicated to handle theoretically. Because of the absence of a clear saddle point on the electronic potential energy surface, the transition state location is also strongly temperature dependent.[62] Moreover, during the process of bond breaking, the system evolves from a singlet state, with the two electrons of the breaking bond in a single molecular orbital, to a triplet state, in which the two electrons move independent from each other in orbitals centered on the formed radicals. To calculate a smooth potential energy surface, a multireference ab initio method is required, which is based on both the singlet and triplet states by expressing the wave function as a weighed superposition of both. Unfortunately, the CBS-QB3 method, which is applied for the other reaction families in this work, is based on single reference calculations. Furthermore, the triple perturbation of CBS-QB3's main CCSD(T) step shows divergent behavior at extended bond lengths. As CBS-QB3 cannot be applied for this reaction family, an alternative was found in the approach of the Klippenstein group, which combines high-level multireference calculations with variable reaction coordinate transition state theory, a variant of energy and angular momentum-resolved VTST[63]:

$$k(T) = \frac{1}{2\pi} g_e \frac{\sigma_A \sigma_B}{\sigma_{\ddagger}} \left(\frac{2\pi}{\mu k_B T}\right)^{3/2} \frac{\int dE dJ\, N^{\ddagger}(E,J) \exp(-E/k_B T)}{Q_A(T) Q_B(T)} \quad (6)$$

In this expression, written in atomic units ($\hbar = 1$), g_e is the electronic degeneracy factor and σ_A, σ_B, and $\sigma_{\ddagger}$ the rotational symmetry numbers for the reactants A and B and the transition state, μ the reduced mass $m_A m_B/(m_A + m_B)$, Q_A and Q_B the reactant partition functions, and $N^{\ddagger}(E,J)$ the E and J resolved density of states of the collision complex. The latter is minimized over the dividing surface for each pair of values of the energy E and the total angular momentum J.

Harding and Klippenstein reported recombination rate coefficients based on second-order multireference perturbation CASPT2/cc-pvdz energies with configuration interaction CAS+1+2/aug-cc-pvtz one-dimensional corrections[64]:

$$V(r,\theta,\varphi) = V_{\text{CASPT2/cc-pvdz}}(r,\theta,\varphi) + \Delta_{\text{CAS+1+2/aug-cc-pvtz}}(r) \quad (7)$$

The one-dimensional corrections $\Delta_{\text{CAS+1+2/aug-cc-pvtz}}(r)$ are determined from the $H + CH_3^{\bullet}$ recombination for hydrogen radical recombinations, and from $CH_3^{\bullet} + CH_3^{\bullet}$ for recombinations between carbon radicals. The reported rate coefficients range from recombinations of hydrogen radicals with alkylic, resonance-stabilized and other radicals[64,65] to recombinations between alkylic radicals.[62] As the reported rate coefficients were not sufficient to cover the 90 recombination reactions considered in this work, the Geometric Mean Rule was used to predict the rate coefficients where possible. The rates for the remaining recombination reactions were assumed to be equal to the rate of structurally similar reactions. An overview of all the recombination reactions, with indication of the source of the value, is given in Table S1 of the Supporting Information.

Sensitivity and rate of production analysis

The complete ab initio reaction network for ethane steam cracking allows to evaluate the main pathways towards the formation of the important products. Furthermore, in every kinetic model, it is useful to know the impact of modifications of certain parameter values. This knowledge can be obtained from a rate of production and sensitivity analysis in commercially available codes such as CHEMKIN 4.1.[66] The one-dimensional plug flow reactor model is applied in combination with the reaction network generated in this work.

The normalized sensitivity coefficients are calculated as follows:

$$\tilde{S}_{ij} = \frac{A_j}{X_i}\frac{\partial X_i}{\partial A_j} = \frac{\partial(\ln X_i)}{\partial(\ln A_j)} \quad (8)$$

In which the effect of the change on the pre-exponential factor A_j of reaction j on the mole fractions X_i of component I is evaluated. For example, a sensitivity coefficient $\tilde{S}_{ij}$ of 0.5 means that a 20% change in $\ln A_j$ (equivalent to a 20% change in $\ln k_j$) will lead to a 10% change in $\ln X_i$. Thus, the magnitude of a sensitivity coefficient is a measure of the effect of the rate coefficient for reaction j on the calculated mole fraction of component i. Clearly, $\tilde{S}_{ij}$ indicates the

importance of reaction step j in determining c_i. Accordingly, a sensitivity analysis provides a way of identifying the most important reaction steps for any particular chemical species of interest.

Note that the reactions are defined as reversible reactions. The consequence of this is that the equilibrium coefficients are kept fixed while changing the rate coefficients. Hence, according to thermodynamic consistency, an increase of the forward rate coefficient k_{forward} with 10% results also in an increase of the reverse rate coefficient k_{reverse}. CHEMKIN reports the normalized sensitivity coefficients based on changes of the forward reaction rate coefficient, thus a positive sign of the normalized sensitivity coefficient implies that the simultaneous increase of the forward and reverse reaction rate coefficient results in an increase of the concentration of the considered species, and a negative sign in a decrease.

Reactors

Pilot Reactor Simulation. The pilot plant installation consists of three parts, see Figure 2: a feed section, the furnace with the suspended reactor coil and the analysis section. The tubular reactor used in this set of experiments is made of Incoloy 800H, has a length of 23.14 m and an internal diameter of 10^{-2} m. These dimensions are chosen to achieve fast turbulent mixing in the coil at the applied feed flow rates. The temperature profile along the reactor is measured and regulated by fired burners. Ethane in B50 cylinders (purity 99.9 vol %) is used as feedstock.

Industrial Reactor Simulation. The geometry of the industrial steam cracker, consisting of a radiation section, a convection section, and an adiabatic cross-over section is given in Figures S1–S3 of the Supporting Information. The details of the geometry, process conditions, reactor equations, and integrating routines can be found in Van Geem et al.[44]

The simulation is performed for the radiation section. The furnace is a rectangular firebox, with four swaged reactor coils suspended in the furnace. Each coil makes eight passes through the furnace. The heat required for the steam cracking of the ethane feed is provided by 128 radiation burners.

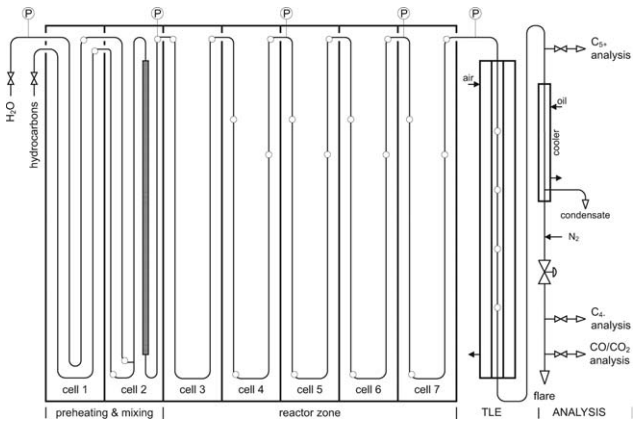

Figure 2. Schematic drawing of the preheating, mixing, and reactor section of the LCT pilot plant installation.

P: pressure measurement, ○: process gas temperature measurement.

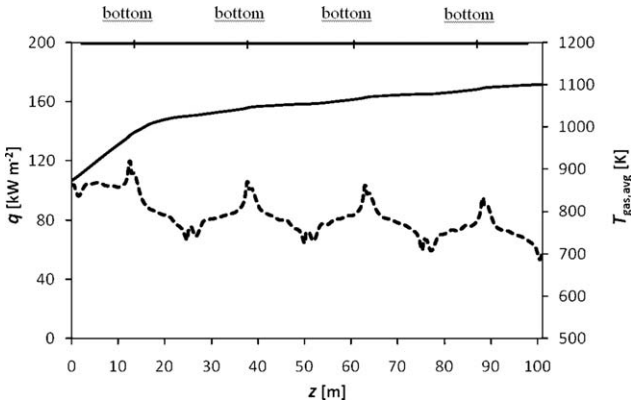

Figure 3. Heat flux profile from furnace to reactor and radial averaged process gas temperature profile (cup mixing temperature, see Eq. 11) as a function of distance in the industrial reactor.

Dotted line: heat flux q, see left axis; full line: temperature, see right axis.

These burners are located in the side walls of the furnace on both sides of the coils, arranged in eight rows of eight burners, see Figures S2 and S3 of the Supporting Information.

The heat flux profile was obtained by performing a coupled simulation of the furnace and the reactor tubes using the two-dimensional reactor model. For the calculation of the furnace, the zone method of Hottel and Sarofim[67] is used. This simulation method is developed by Vercammen and Froment,[68] Rao et al.,[69] and Plehiers and Froment,[70] and consists of iteratively solving the furnace enthalpy balance and simulating the reactor coil, both linked by the profile of the heat flux into the coils, until convergence is reached. The resulting heat flux, given in Figure 3, is strongly non-uniform due to the non-uniformity of the fuel gas temperatures in the furnace. At the top of the furnace the heat flux is much lower than at the bottom, where there are sharp peaks, since there are no burners in the top section of the furnace.

The furnace and reactor geometry characteristics are listed in Table 3. The total hydrocarbon flow rate through one reactor coil is 0.972 kg/s. The inlet temperature of the process gas is 873 K. During the steam cracking of ethane a steam dilution of 0.35 kg/kg feed is applied. The steam reduces the partial pressure of the hydrocarbons in the gas phase and reduces coke formation. As can be seen from Table 3, the ethane feed contains 0.90 wt % ethene and 1.40 wt % of propene as impurities.

The operating conditions for the steam cracking furnace are listed in Table 4. The total fuel gas flow for the 128 burners is 0.559 kg/s. The total amount of heat provided by the burners is 28 MW. The excess of air is 2%, since the chance of incomplete combustion is rather limited with the fuel gas consisting mainly of methane.

Results and Discussion

Reaction network

The reaction network consists of 1512 reversible reactions between 129 species, that is, 92 radical and 37 molecular

Table 3. Furnace, Reactor Geometry, and Process Conditions for the Standard Industrial Ethane Cracking Furnace

Furnace	
Furnace length	9.30 m
Furnace height	13.45 m
Furnace width	2.10 m
Thickness refractory material	0.23 m
Thickness insulation material	0.05 m
Number of burners	128
Heat input	14.43 MW
Reactor coil	
Number of reactors	4
Number of passes	8
Reactor length	100.96 m
Reactor diameter (int)	0.124 m
Wall thickness	0.008 m
Ethane flow rate per reactor coil	0.972 kg/s
Steam dilution	0.35 kg/kg
Coil inlet temperature	873 K
Coil inlet pressure	3.4×10^5 Pa
Coil outlet pressure	1.8×10^5 Pa
Composition of the feed	
Ethane	97.70 wt %
Ethene	0.90 wt %
Propene	1.40 wt %

species with maximally eight carbon atoms (see Supporting Information for the reaction network in CHEMKIN format).[45] The majority of these 1512 reactions are hydrogen abstractions reactions, that is, 1302 hydrogen abstractions, and furthermore 90 radical recombination/bond scissions and 120 Radical addition/β scissions are present. The network also includes intramolecular reactions, with four intramolecular H-abstractions and 12 intramolecular radical additions. The reaction rates for the forward reaction are calculated as described in the methodology section. The reaction rates for the reverse reactions are calculated using thermodynamic consistency.

To check the reliability of the extensive network it is compared to a rate-based generated network using the ab initio thermodynamic and kinetic data only. Rate-based termination of computer-generated reaction networks provides a physicochemical criterion for including reactions and species[15,50,71]; only those pathways whose rates exceed some minimum rate criterion, R_{min}, are included in the network. Hence, the ab initio-based thermodynamics and reaction rate parameters determine which reaction paths are included and which are not. In this work, the Reaction Mechanism Generator (RMG 2.0) is applied for the rate-based generation.[8,11,72] The reaction conditions used for generating the ethane steam cracking model with RMG are a fixed temperature of 1100 K, a fixed pressure of 2.0×10^5 Pa, with an initial ethane concentration of 1.0 mol/m^3. The error tolerance is set to 0.02, while a conversion of 75% is used, corresponding to the highest conversion observed during the ethane cracking experiments. The RMG generated reaction network consists of 1517 reversible reactions between 129 species, that is, 98 radical and 31 molecular species with maximally eight carbon atoms. A comparison with reference data for ethane pyrolysis and steam cracking shows that all expected products and intermediates are included in the rate-based reaction network, even pathways to benzene, toluene, and styrene. The latter is a first indication that the ab initio thermodynamics and kinetics allow to generate a reliable reaction network.

The extensive reaction network, generated using the carbon count stop criterion,[45] and the RMG generated reaction network are very similar. All the species and 99% of the reactions included in the RMG generated network are accounted for in the extensive network. This is because of the very loose error tolerances applied for the RMG generated network, using stricter tolerances results in smaller networks but not all observed products are accounted for.

Pilot plant simulation

To verify if the reaction network with ab initio thermodynamics and kinetics allows to obtain accurate simulation results without adjusting kinetic or thermodynamic parameters, a set of pilot plant experiments is simulated. This experimental pilot plant setup at the Laboratory for Chemical Technology allows fundamental studies of the kinetics of the cracking reactions[73] as well as of practical issues such as coke deposition in both the radiant coil[74] and the transfer line exchanger (TLE).[75]

The extensive reaction network is used to simulate eight pilot plant experiments. The feed flow rate of the ethane feedstock in the experiments, F_0, is varied from 0.9×10^{-3} to 1.1×10^{-3} kg/s, while the coil outlet temperature, COT, varies from 1063 K to 1163 K. The dilution varies from 0.25 kg steam/kg ethane to 0.6 kg steam/kg ethane. The coil outlet pressure, COP, varies from 0.17 MPa to 0.21 MPa. These conditions correspond with ethane conversions ranging from 10 to 75%.

The results in Tables 5 and 6 for two experiments at a similar conversion but with a different dilution show the good agreement between simulation results and experimental data. The ethane and ethene yields are predicted within 5% of the experimental yields, and the yields of the other products (>0.50 wt %) are within 15% of the experimental yields

Table 4. Furnace Operating Conditions

Fuel gas composition (mol %)	
Nitrogen	0.71
Hydrogen	0.50
Carbon dioxide	0.28
Methane	96.27
Ethane	0.93
Ethene	0.77
Propane	0.32
Propene	0.03
n-Butane	0.095
i-Butene	0.095
Fuel gas composition (mol %)	
Nitrogen	70.39
Oxygen	0.37
Carbon dioxide	9.27
Water	19.97
Furnace operation	
Air excess (%)	2
Fuel gas flow (kg/s)	5.59×10^{-1}
Flue gas flow (mol/mol)	10.98
Adiabatic flame temperature (K)	2277
Burner cup temperature (K)	1631
Fuel gas inlet temperature (K)	2073

Table 5. Comparison Between Simulated Pilot Plant Product Yields (wt %) and Experimental Data

	COILSIM1D		
	Simulated Ab Initio	Simulated CRACKSIM	Experimental
Hydrogen	4.12	3.92	3.90
Methane	1.82	3.01	3.11
Ethyne	1.00	0.81	0.89
Ethene	51.77	50.18	49.87
Ethane	38.03	38.55	38.75
Propyne	0.03	0.04	0.04
1,2-Propadiene	0.02	0.02	0.01
Propene	0.51	0.81	0.80
Propane	0.04	0.09	0.09
1,3-Butadiene	1.47	1.30	1.40
1-Butene	0.07	0.12	0.12
Butane	0.09	0.30	0.34
1,3-Cyclopentadiene	0.11	0.09	0.12
Benzene	0.61	0.59	0.60

Conditions: $F_0 = 0.92$ g/s, $\delta = 0.583$ kg/kg, COT = 1101 K, COP = 1.91×10^5 Pa.

except for methane and propene, and for the second simulation also ethyne. The overall good agreement is remarkable because none of the kinetic parameters used for obtaining the simulation results were fitted to the experimental data. However, the agreement with experiment is not as good as the one obtained using CRACKSIM.[45] CRACKSIM contains the same reaction network but the reaction rate coefficients have been fitted to an extensive set of reference pilot plant experiments which explains the good agreement. The CRACKSIM/COILSIM1D product yields (>0.50 wt %) are within 10% of the experimental yield except for ethyne, similar to the use of ab intio kinetics.

In Figure 4, the ethane conversion profile is shown for the pilot plant experiment at the conditions of Table 5. The ethane conversion profile shows an induction period corresponding with the heating of the process gasses to the reaction temperature. Once the quench zone is reached, the reaction stops rapidly and the conversion remains fixed. Also, for other temperature profiles, dilutions, and COP's, the conversion is accurately simulated, as can be seen from

Table 6. Comparison Between Simulated Pilot Plant Product Yields (wt %) and Experimental Data

	COILSIM1D		
	Ab Initio Kinetics	CRACKSIM Fitted Kinetics	Experimental
Hydrogen	3.89	3.66	3.64
Methane	1.80	3.36	3.15
Ethyne	0.76	0.67	0.59
Ethene	49.42	47.82	48.12
Ethane	40.98	40.98	40.36
Propyne	0.03	0.04	0.03
1,2-Propadiene	0.01	0.01	0.01
Propene	0.55	0.80	0.79
Propane	0.05	0.12	0.13
1,3-Butadiene	1.38	1.42	1.29
1-Butene	0.06	0.11	0.12
Butane	0.09	0.20	0.26
1,3-Cyclopentadiene	0.09	0.07	0.07
Benzene	0.51	0.48	0.44

Conditions: $F_0 = 1.03$ g/s, $\delta = 0.267$ kg/kg, COT = 1111 K, COP = 1.90×10^5 Pa.

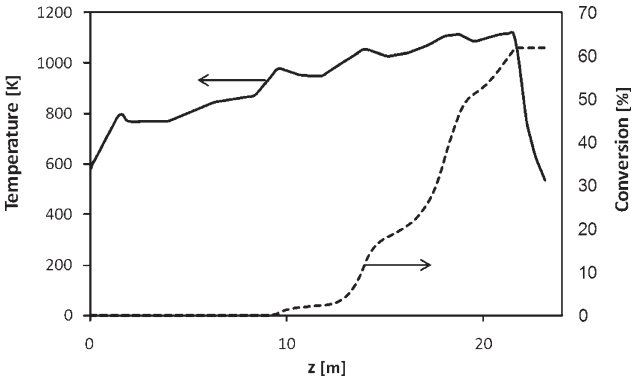

Figure 4. Simulated ethane conversion profile (dotted line) and the measured process gas temperature profile imposed at the simulation (full line) for an ethane pilot plant experiment.

Conditions: $F_0 = 0.92$ g/s, $\delta = 0.583$ kg/kg, COT = 1101 K, COP = 1.91×10^5 Pa.

Figure 5, even under severe cracking conditions and high steam dilutions. The latter is also the case for the ethene yield, although a slight tendency to overpredict the ethene yield can be observed in Figure 5. A typical pressure profile can be found in Figure S4 of the Supporting Information.

The product yields for the minor products are also predicted satisfactorily, as can be observed in Figure 6. The predicted yields for hydrogen, ethyne, 1,3-butadiene, and benzene are in the 10% error interval at almost all experimental conditions. Only the methane and propene yields are significantly underestimated by 40–50% for methane and by 30–60% for propene.

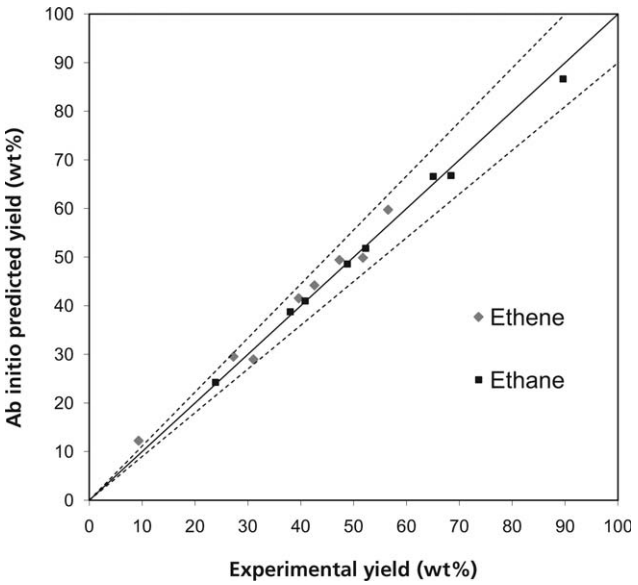

Figure 5. Ab initio predicted vs. experimental product yields for ethane and ethene in the pilot plant simulation.

Conditions: $F_0 = 0.9–1.1$ g/s, $\delta = 0.25–0.6$ kg/kg, COT = 1063–1163 K, COP = $1.7–2.1 \times 10^5$ Pa; [- - - 10% rel. interval].

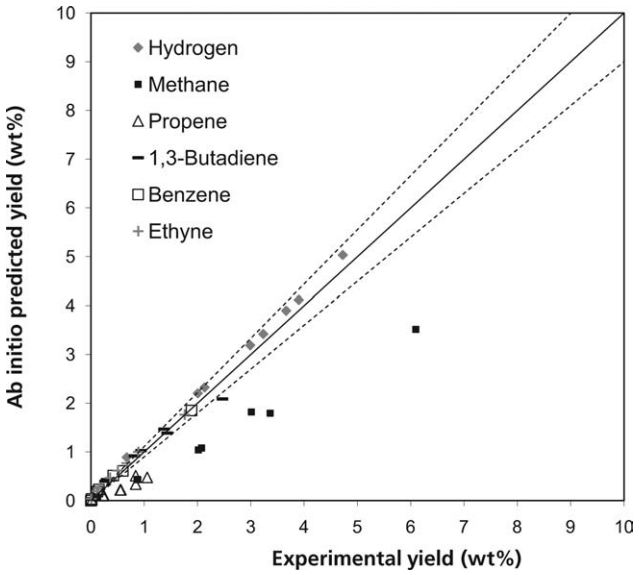

Figure 6. Parity plot for minor products: hydrogen, methane, ethyne, propene, 1,3-butadiene, and benzene.

Conditions: F_0 = 0.9–1.1 g/s, δ = 0.25–0.6 kg/kg, COT = 1063–1163 K, COP = 1.7–2.1 × 10^5 Pa, [- - - 10% rel. interval].

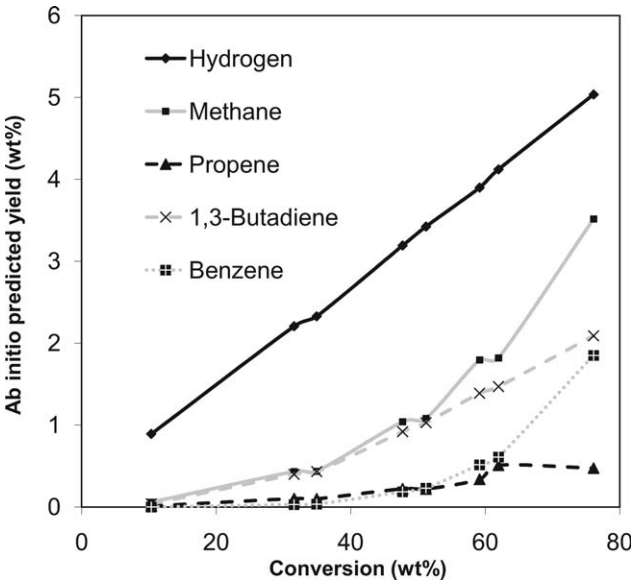

Figure 7. Ab initio predicted product yields of the minor products (hydrogen, methane, ethyne, propene, 1,3-butadiene, and benzene) vs. the ethane conversion.

Conditions: F_0 = 0.9–1.1 g/s, δ = 0.25–0.6 kg/kg, COT = 1063–1163 K, COP = 1.7–2.1 × 10^5 Pa.

The results in Figure 7 show that for the minor products the expected trends as function of the conversion are obtained. All yields increase with increasing conversion, with methane having the strongest increase, and the propene yield has a maximum as expected. Note that the product yields in Figure 7 pertain to experiments at different dilutions explaining the discontinuous curves for product yields as function of conversion.

To gain more insight into which reaction paths are dominant and thus responsible for the inaccuracies for propene and methane formation and the accurate prediction of the other product yields, a sensitivity and rate of production analysis is performed. The analysis is performed for the experiment shown in Figure 4, that is, the temperature and pressure profile are those measured in the pilot plant.

Table 7 presents the normalized sensitivity coefficients of the major products at the reactor inlet and at the reactor outlet, for the five reactions with the largest sensitivity coefficient $\tilde{S}_{ij}$, as given by Eq. 8. Positive values for the sensitivity coefficients indicate a concentration increase in propene with increasing rate coefficient and vice versa. The different sensitivities at the beginning and end of the reactor for the same rate coefficient are mainly due to differences in temperature and concentrations of the reactants and products.

From the results of the rate of production analysis and the normalized sensitivity coefficients for propene in Table 7, it follows that the too low propene yield is mainly caused by the too fast hydrogen addition reactions to propene. The resulting primary propyl radical rapidly decomposes to ethene:

$$H^{\bullet} + C_3H_6 \rightleftharpoons C_3H_7^{\bullet}(p) \tag{9}$$

$$C_3H_7^{\bullet}(p) \rightleftharpoons CH_3^{\bullet} + C_2H_4 \tag{10}$$

Replacing the ab initio calculated kinetic parameters for the H addition to propene (k = 4.6 × 10^6 m^3/mol/s at 1000 K) with those proposed by Curran[76] based on a meta-analysis of the available experimental data (k = 2.3 × 10^6 m^3/mol/s) results in an increase of the propene yield with 50%. This difference in rate coefficient could be caused by pressure dependence, similar to the hydrogen addition to ethene.[77]

On the basis of the sensitivity analysis, the main reason for the observed differences for the methane yield is the competition between hydrogen abstractions from ethane by the hydrogen radical (reaction 2 in Table 7) and by the

Table 7. Sensitivity Coefficients at the Beginning of the Pilot Reactor and at the Reactor Outlet

		Beginning of Reactor				End of Reactor			
		/	//	CH_4	///	/	//	CH_4	///
1	$C_2H_6 \iff CH_3^{\bullet} + CH_3^{\bullet}$	0.05	0.65	1.00	1.95	−0.18	0.08	0.85	0.74
2	$H^{\bullet} + C_2H_6 \iff H_2 + C_2H_5^{\bullet}$	0.05	0.18	–	−0.80	−0.31	0.20	−0.26	−0.03
3	$2\ C_2H_5^{\bullet} \iff C_4H_{10}$	0.04	−0.33	–	−0.02	0.08	−0.05	0.09	1.42
4	$C_2\ H_5^{\bullet} \iff C_2H_4 + H^{\bullet}$	0.04	0.99	–	0.84	−0.04	0.02	−0.05	−0.02
5	$H^{\bullet} + C_3H_6 \iff 1 - C_3H_7^{\bullet}$	–	–	–	0.04	–	–	0.03	−0.17

Conditions: F_0 = 0.92 g/s, δ = 0.583 kg/kg, COT = 1101 K, COP = 1.91 × 10^5 Pa.

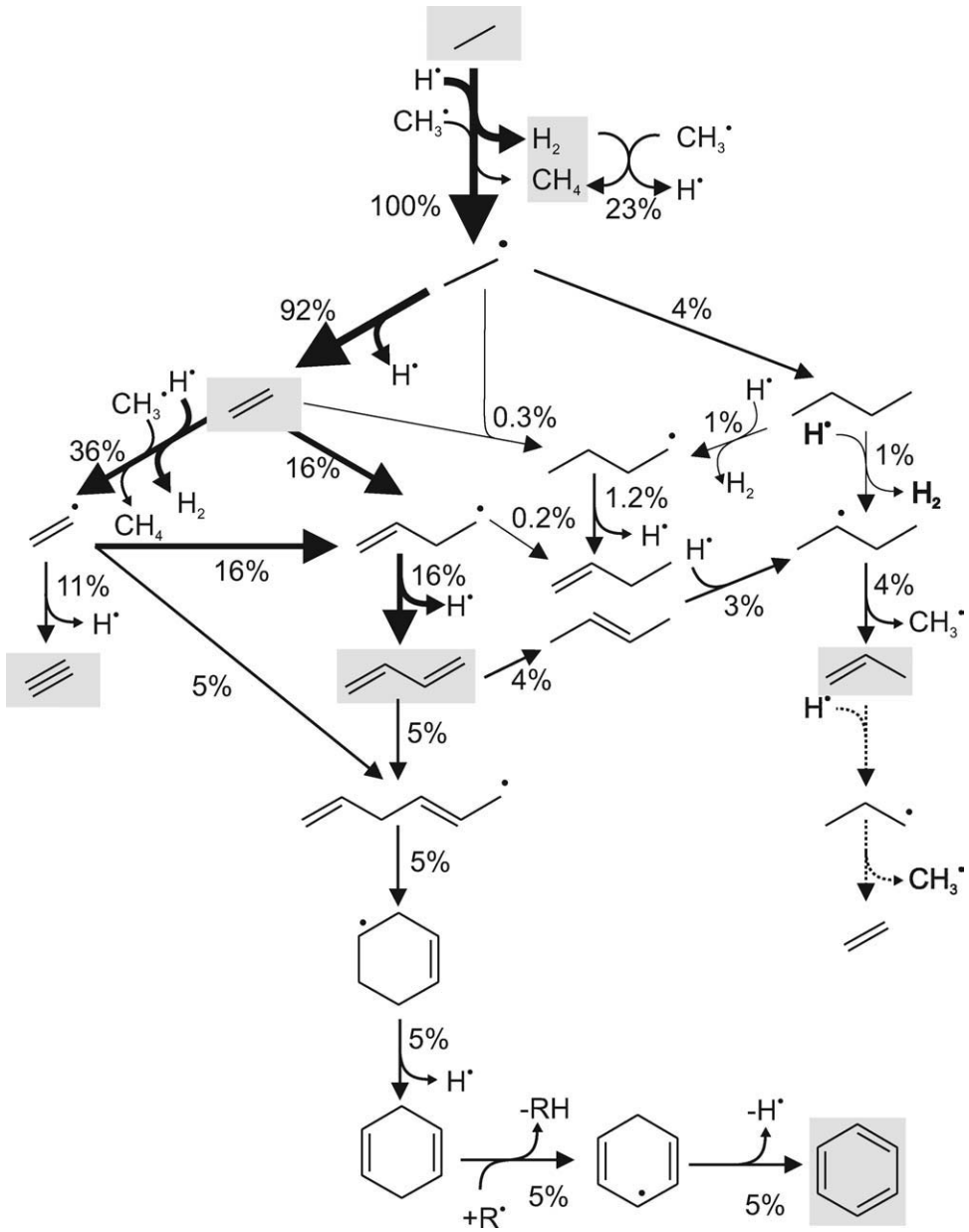

Figure 8. Reaction pathway analysis for ethane decomposition towards the main products (gray shaded boxes), performed at the maximum temperature along the reactor coil.

The arrow thickness and percentages represent the reaction rate relative to the total ethane decomposition rate. $R^{\bullet}$ is, in order of importance, the $H^{\bullet}$, $C_2H_3^{\bullet}$, $CH_3^{\bullet}$, $C_2H_5^{\bullet}$, and $C_4H_5^{\bullet}$ radical. The dotted lines indicate the propene decomposition discussed in the text. (Axial position 21.56 m, $T = 1151.5$ K. Reactor conditions: $F_0 = 0.92$ g/s, $\delta = 0.583$ kg/kg, COT = 1101 K, COP = 1.91×10^5 Pa).

methyl radical. The hydrogen abstractions by hydrogen are so fast that the abstractions by methyl radicals, which form the main source of methane, have difficulties to compete (7.9×10^3 m^3/mol/s for the abstraction by $CH_3^{\bullet}$ from ethane at 1000 K, compared to 1.1×10^6 m^3/mol/s for the abstraction by $H^{\bullet}$).

The results of the rate of production analysis are summarized in the reaction pathways of Figure 8 for the pathways to the main products. The analysis in Figure 8 is performed at the point in the reactor with the maximum temperature just upstream of the coil outlet (1151.5 K), corresponding to a maximum formation of side products. At this point in the reactor the radical concentration is high (0.016 wt %), and radical formation steps can be omitted.

Though the highest rate of production of ethene, the primary product, occurs earlier in the reactor coil, ethene is at the end of the reactor still the dominantly formed product. The first step in ethane conversion, the formation of the ethyl radical, occurs predominantly via hydrogen abstraction by the abundantly present hydrogen radical. Other radicals contribute less than 10% to the ethane conversion.

The formed ethyl radical decomposes for 92% into ethene by a C-H β scission. The remaining 8% mainly recombines with other radicals, the self-recombination to *n*-butane being

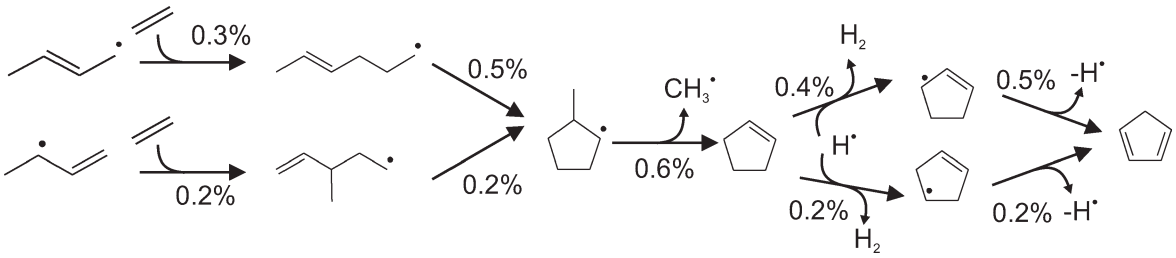

Figure 9. Reaction pathway analysis for cyclopentadiene formation, performed at the maximum temperature along the reactor coil.

The percentages represent the reaction rate relative to the total ethane decomposition rate. (Axial position 21.56 m, $T = 1151.5$ K. Reactor conditions: $F_0 = 0.92$ g/s, $\delta = 0.583$ kg/kg, COT = 1101 K, COP = 1.91×10^5 Pa).

the most significant one with 4%, since it immediately decomposes to propene and butene.

The rate coefficient for the C-H β scission producing ethene is calculated from the reverse reaction, the hydrogen addition to ethene. Hydrogen additions to unsaturated molecules are significantly faster than addition reactions involving other radicals, such as methyl radicals. From the comparison between ab initio and experimental rates given in Sabbe et al.[29] it can be observed that the rate coefficient for the H addition to ethene is about 60% faster than the experimentally observed value at 1000 K. As this reaction determines the reverse β scission, this could explain the slight overprediction of the ethene yield. All rate coefficients have been calculated in the high pressure limit, and therefore pressure dependence for this reaction can be the reason for the observed differences. The overprediction of rate coefficients could indeed be attributed to pressure dependence, as suggested by Miller and Klippenstein.[77] Using a master equation analysis for the hydrogen addition to ethene in He as bath gas, they showed that this reaction has just reached the high pressure limit at 298 K, from which can it be expected that the reaction is pressure dependent at the higher temperatures of steam cracking. Also, hydrogen abstractions by hydrogen radicals are slightly faster than experimental values, which can explain the systematic overprediction of the hydrogen yield as observed in Figure 6.

At the elevated temperatures at the end of the coil, more than half of the ethene formed is further converted, mainly into vinyl radicals (36% with respect to the ethane disappearance rate) and the but-1-en-4-yl radical (16%), the main precursor for 1,3-butadiene. The but-1-en-4-yl radical is formed by addition of vinyl radicals to ethene, which consumes almost half of the vinyl radicals formed. The other half mainly decomposes by C-H β scission to ethyne or adds to 1,3-butadiene to initiate the main path towards benzene.

Under steam cracking conditions, the addition of vinyl radicals to 1,3-butadiene and the subsequent cyclization and dehydrogenation is the dominant path towards benzene formation. The reaction path shown is responsible for 80% of the total benzene production. This pathway to benzene does not agree with the one proposed by Matheu and Grenda.[78] These authors found that in their reaction network generated for a similar temperature range but lower pressure (900–1200 K and 4.0×10^4 Pa) the recombination of propargyl radicals was the main pathway to benzene for ethane pyrolysis. In this work, using the recombination rate coefficients reported by Miller and Klippenstein,[79] the recombination of propargyl radicals does not contribute significantly according to a rate of production sensitivity analysis. It only starts contributing to the benzene rate of formation at a temperature of 1130 K. The C_3H_3 recombination reaction path can even be omitted from the reaction network without any loss of accuracy.

A similar path initiates the formation of 1,3-cyclopentadiene with the addition of the but-1-en-3-yl radical to ethene (see Figure 9). Although a significant amount of 1,3-cyclopentadien-5-yl is formed, recombination reactions of the methyl radical with 1,3-cylopentadien-5-yl radicals do not seem to be contributing to the benzene yield during the cracking of ethane under the specified conditions. This reaction, via the intermediate fulvene, is sometimes considered as one of the important pathways towards benzene formation in combustion and pyrolysis.[80,81]

The dominant reaction pathway to methane (99% of the production) is the hydrogen abstraction reaction by methyl radicals. In the first part of the reactor, the hydrogen is clearly abstracted from ethane, but in the last part, with already many of the ethane feed converted, mainly from dihydrogen and to a lesser extent ethene. From the reaction pathway analysis in Figure 8 it is clear that at the end of the reactor coil the major contribution to methane formation is the abstraction from the dihydrogen formed in the first step of ethane decomposition.

The formation of propene occurs, next to a small contribution from recombinations of allyl and prop-1-en-2-yl radicals with hydrogen radicals, by the C-C β scission of but-2-yl radicals, releasing a methyl radical. This but-2-yl radical originates from various sources, mainly hydrogen addition to 1 and 2-butene and hydrogen abstraction from *n*-butane. The butenes are formed by a series of hydrogen additions and abstractions from 1,3-butadiene (not shown in detail).

Despite the underpredictions of propene and methane, which are most possibly caused by too reactive hydrogen radicals, the overall ab-initio only prediction remains impressive. The successful reactor simulation shows that ab initio methods in combination with an engineering approximation, such as the group additive method, are a useful tool in reactor simulations. Furthermore, since none of the applied kinetic parameters has been fitted to experimental data, no deficiencies in the network could be obscured. Therefore, it can be inferred from the quantitative agreement to experimental product that the reaction network is complete and describes all the relevant chemistry during the cracking of ethane.

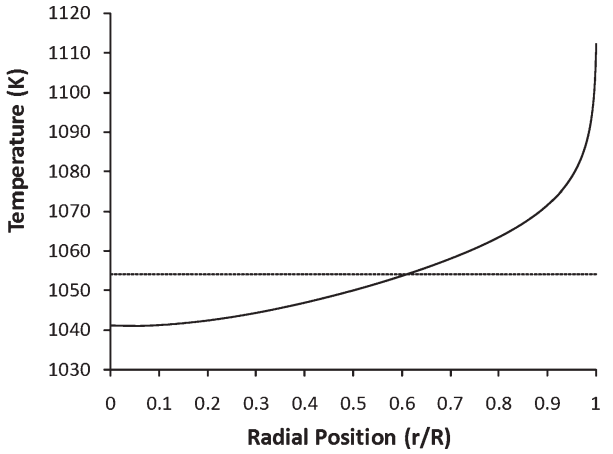

Figure 10. Radial temperature profile at an axial position of 50 m in the industrial coil for the ab initio COILSIM2D simulation.

Full line: 2D model, dotted line: cup-mixing temperature.

Industrial reactor simulation

For the industrial cracking reactor, the 2D approach is justified by the important radial temperature gradients in the reactor, as can be observed in the profile in Figure 10. This results in radially varying concentration profiles for the considered species. For the calculation of the average process gas temperature for the two-dimensional reactor model, the cup mixing equation is applied[82]:

$$T_{\mathrm{av}} = \frac{\int_0^R T(r)u(r)rdr}{\int_0^R u(r)rdr} \tag{11}$$

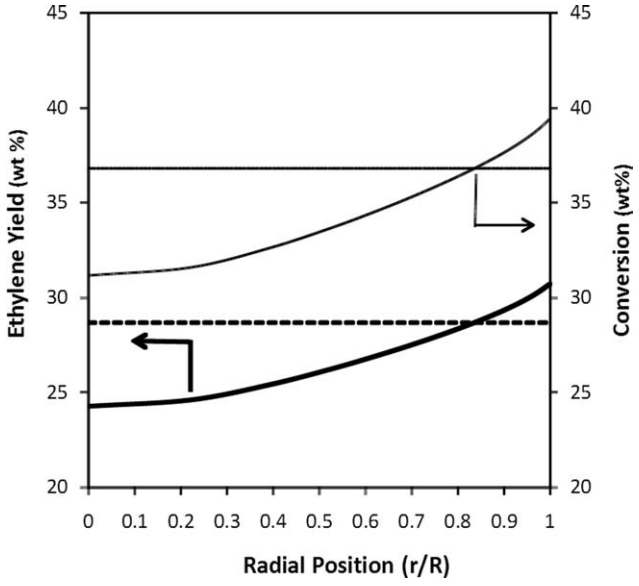

Figure 11. Ab initio simulated conversion and ethene yield as a function of radial position at an axial position of 75 m; ——— ethylene yield 2D; — — — ethylene yield 1D; – – – – ethane conversion 2D; - - - - - - ethane conversion 1D.

Table 8. Comparison Between Simulated Product Yields (wt %) and Experimental Data for an Industrial Ethane Cracker

	COILSIM2D		
	Ab Initio Kinetics	CRACKSIM Fitted Kinetics	Industrial
Hydrogen	3.10	3.02	3.06
Methane	3.00	4.24	2.20
Ethyne	0.30	0.28	N.A.
Ethene	42.21	41.20	41.50
Ethane	48.32	48.46	48.85
Propyne	0.02	0.03	N.A.
Propadiene	0.02	0.01	N.A.
Propene	0.60	0.89	0.89
1,3-Butadiene	1.16	1.10	0.58
1-Butene	0.11	0.16	N.A.
1,3-Cyclopentadiene	0.13	0.15	N.A.
Benzene	0.40	0.34	0.30

Figure 11 shows clearly the varying radial ethane conversion and the ethene yield over a cross section at an axial position of 75 m. The higher conversion near the wall results in a higher ethene yield in this zone. The higher conversion in this zone will also affect the yields of other products.

The simulated product yields of the important cracking products are given in Table 8, in comparison to industrial data and CRACKSIM simulated data. The industrial data refer to the recovered products after the separation steps. As these data are not as reliable as the data obtained using the analysis section of the pilot plant, a bias on the comparison of the ab initio simulated product yields at the end of the reactor and the industrially recovered products can be expected. Comparison with the industrial data shows that a remarkably good agreement is obtained taking in to account that none of the kinetic or thermochemical data were adjusted to improve the fit. The main differences are found for methane, propene, and 1,3-butadiene. Methane yields are too high for this simulation, compared to too low yields for the pilot plant simulations. In the industrial reactor simulation, the methane yield is very sensitive to the H addition to propene (reaction 2 in Figure 12) due to the presence of 1.4 wt % propene impurity in the feed. As the hydrogen additions are slightly too fast, this could cause the methane overprediction. The pressure dependence of the rate coefficients is, however, expected to be smaller than in the pilot plant simulations because of the higher operating pressures.

Comparing the simulated yields using CRACKSIM with the industrial data shows that a better agreement is obtained for ethane, ethane, and propene. But CRACKSIM overestimates 1,3-butadiene as much as when using the ab initio kinetics, and even predicts a higher methane yield than the one obtained using the ab initio kinetics.

Conclusions

This work presents the application of a first principle-based group additive method for the calculation of thermodynamics and Arrhenius parameters involved in the radical chemistry of hydrocarbons. The consistently developed group additive model is applied in the simulation of an ethane steam cracker, in contrast to the usually applied combination of

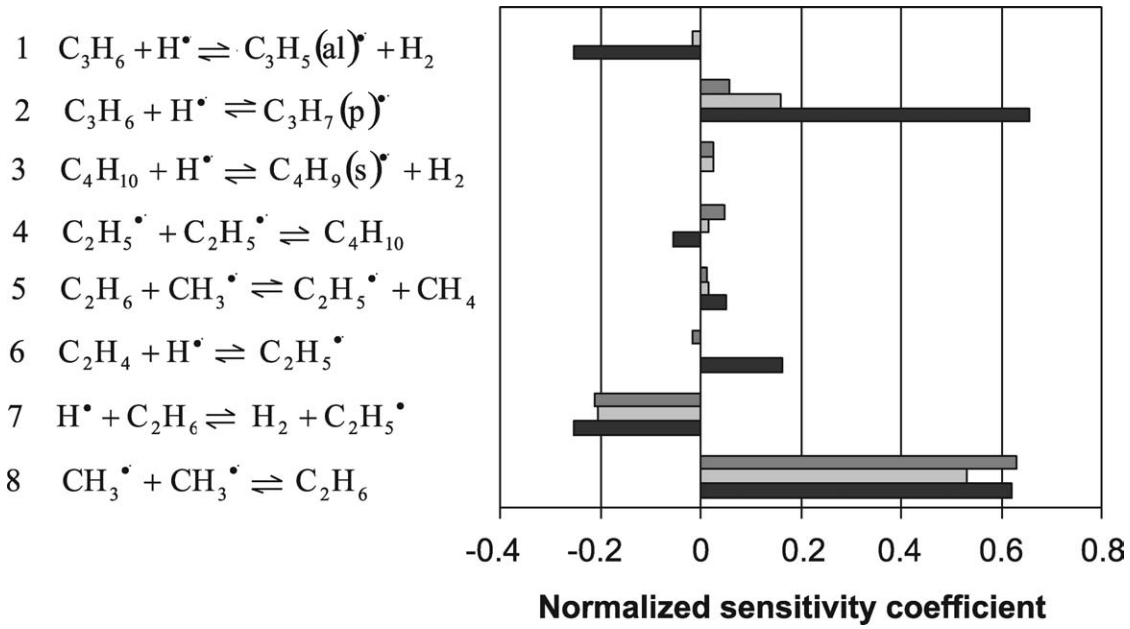

Figure 12. Normalized sensitivity coefficients for methane at the beginning of the reactor (dark gray), in the middle of the reactor (light gray), and at the reactor outlet (black) for the simulation of an industrial reactor.

experimentally determined, predicted and fitted data. By using only these ab initio-based additive models, the product yields for a pilot and industrial cracker can be simulated within 15% except for the methane and propene yields. As no parameter has been adjusted and no experimental values have been used, the agreement can be considered remarkable. To the best of our knowledge, this is the first full ab initio simulation of an industrial chemical reactor. The observed differences in product yields can be largely attributed to a few hydrogen addition reactions that seem to be too fast. Pressure dependence, which is currently neglected, probably needs to be taken into account for these reactions.

The full ab initio simulation has shown that the vast majority of the benzene is formed via a pathway initiated by vinyl radical addition to 1,3-butadiene, and subsequent cyclization and dehydrogenation. Propargyl radical recombination, which is sometimes advocated to be the main pathway towards benzene under pyrolysis conditions, plays only a marginal role under steam cracking conditions.

From the successful simulation of an industrial ethane cracker, several conclusions can be drawn. First, the success of the simulation delivers a proof-of-principle that the integration of computational chemistry methods with engineering tools at larger time and length scales provides a predictive tool that can be used for the design and optimization of industrial chemical processes. The methodology developed in this work is able to provide radical reaction networks with reliable kinetic and thermodynamic data and requires no adjustable parameters nor direct experimental data. Second, because of the absence of fitted data that could compensate for possible deficiencies in the reaction network, it has been shown that the reaction network is complete, in the sense that it describes all the relevant chemistry occurring under steam cracking conditions.

Although the data obtained in this work cover only hydrocarbon radical gas phase reactions, the rate coefficients obtained using the developed ab initio-based group additivity methods represent the intrinsic chemical kinetics of the reactions and, hence, are independent of the studied process. Therefore, the developed group additive models can be applied in other reaction networks as well, including the description of hydrocarbon reactions in reaction networks including hetero atoms. The application range of the group additive models developed in this work covers processes based on gas phase radical chemistry, such as radical polymerization processes, partial oxidation, and pyrolysis processes.

The final conclusion is that ab initio methods can be considered a feasible tool for the modeling of chemical processes based on gas phase radical chemistry. The simulation of a chemical reactor built on ab initio calculations and kinetic models only, without a single adjusted parameter or experimental value, is within the reach of the current methods. The challenge now is to extend this work to more complex processes, and to apply similar methodologies to unexplored reaction conditions and feeds, as well as novel processes.

Acknowledgments

M.K.S. held a Ph.D. grant of the Institute for the Promotion of Innovation through Science and Technology in Flanders (IWT-Vlaanderen) and is currently Postdoctoral Fellow of the Fund for Scientific Research, Flanders, Belgium. K.M. Van Geem holds a Postdoctoral Fellowship of the Fund for Scientific Research, Flanders, and a Fulbright fellowship for performing postdoctoral research at the Massachusetts Institute of Technology.

Notation

Acronyms

CAS = complete active space
CIT = coil inlet temperature
COP = coil outlet pressure
COT = coil outlet temperature

Roman letters

A = pre-exponential factor (m^3/mol/s or s^{-1})
$\tilde{A}$ = single-event pre-exponential factor (m^3/mol/s or s^{-1})
$\tilde{A}_{ref}$ = single-event pre-exponential factor of the reference reaction (m^3/mol/s or s^{-1})
d_t = internal tube diameter (m)
E = electronic energy (kJ/mol)
E_a = activation energy (kJ/mol)
$E_{a,ref}$ = activation energy of reference reaction (kJ/mol)
F_0 = initial total mass flow (kg/s)
F_j = molar flow rate (mol/s)
ΔGAV° = kinetic group additive value relative to reference reaction (kJ/mol, m^3/mol/s, or s^{-1})
$\Delta_r G^\circ$ = standard reaction Gibbs energy (kJ/mol)
$\Delta_f H^\circ$ = standard enthalpy of formation (kJ/mol)
J = total angular momentum quantum number
k = rate coefficient (m^3/mol/s or s^{-1})
K = equilibrium coefficient (m^3/mol or N density of states, –)
n_e = number of single events (–)
n_{opt} = number of optical isomers (–)
p = pressure (Pa)
p_t = total pressure (Pa)
Q = partition function (–)
r = radial coordinate (m)
R = radius of the tube (m)
r_k = rate of reaction k (mol/m^3/s)
S_{ij} = normalized sensitivity coefficient (–)
S° = standard entropy (J/mol/K)
T = temperature (K)
X = mole fraction (–)
z = axial coordinate (m)

Greek letters

$\ddagger$ = transition state (–)
ρ = factor of deviation between rate coefficients (–)
δ = steam to hydrocarbon dilution (kg/kg)
μ = reduced mass (kg)
σ = symmetry number (–)

Literature Cited

1. Molina MJ, Molina LT, Kolb CE. Gas-phase and heterogeneous chemical kinetics of the troposphere and stratosphere. *Annu Rev Phys Chem*. 1996;47:327–367.
2. Rowland FS. Stratospheric ozone depletion by chlorofluorocarbons (Nobel lecture). *Angew Chem Int Ed Eng*. 1996;35:1786–1798.
3. Simpson WR, von Glasow R, Riedel K, Anderson P, Ariya P, Bottenheim J, Burrows J, Carpenter LJ, Friess U, Goodsite ME, Heard D, Hutterli M, Jacobi HW, Kaleschke L, Neff B, Plane J, Platt U, Richter A, Roscoe H, Sander R, Shepson P, Sodeau J, Steffen A, Wagner T, Wolff E. Halogens and their role in polar boundary-layer ozone depletion. *Atm Chem Phys*. 2007; 7:4375–4418.
4. Ge MF, Ma CP. Reactive halogen chemistry. *Progr Chem*. 2009;21: 307–334.
5. Sundaram KM, Froment GF. Comparison of simulation-models for empty tubular reactors. *Chem Eng Sci*. 1979;34:117–124.
6. Dente M, Ranzi E, Goossens AG. Detailed prediction of olefin yields from hydrocarbon pyrolysis through a fundamental simulation-model (Spyro). *Comput Chem Eng*. 1979;3:61–75.
7. Clymans PJ, Froment GF. Computer-generation of reaction paths and rate-equations in the thermal-cracking of normal and branched paraffins. *Comput Chem Eng*. 1984;8:137–142.
8. Green WH. Predictive kinetics: a new approach for the 21st century. *Adv Chem Eng*. 2007;32:1–50.
9. van Goethem MWM, Kleinendorst FI, van Leeuwen C, van Velzen N. Equation-based SPYRO (R) model and solver for the simulation of the steam cracking process. *Comput Chem Eng*. 2001;25:905–911.
10. Bos ANR, Lefferts L, Marin GB, Steijns MHGM. Kinetic research on heterogeneously catalyzed processes: a questionnaire on the state-of-the-art in industry. *Appl Catal A Gen*. 1997;160: 185–190.
11. Van Geem KM, Reyniers MF, Marin GB, Song J, Matheu DM, Green WH. Automatic reaction network generation using RMG for steam cracking of n-hexane. *AIChE J*. 2006;52:718–730.
12. Rice FO, Herzefeld KF. The thermal decomposition of organic compounds from the standpoint of free radicals VI. The mechanism of some chain reactions. *J Am Chem Soc*. 1934;56:284–289.
13. Ranzi E, Dente M, Plerucci S, Biardi G. Initial product distributions from pyrolysis of normal and branched paraffins. *Ind Eng Chem Fund*. 1983;22:132–139.
14. Hillewaert LP, Dierickx JL, Froment GF. Computer generation of reaction schemes and rate equations for thermal cracking. *AIChE J*. 1988;34:17–24.
15. Broadbelt LJ, Stark SM, Klein MT. Computer generated reaction modeling: decomposition and encoding algorithms for determining species uniqueness. *Comput Chem Eng*. 1996;20:113–129.
16. Battin-Leclerc F, Glaude PA, Warth V, Fournet R, Scacchi G, Come GM. Computer tools for modeling the chemical phenomena related to combustion. *Chem Eng Sci*. 2000;55:2883–2893.
17. Wauters S, Marin GB. Computer generation of a network of elementary steps for coke formation during the thermal cracking of hydrocarbons. *Chem Eng J*. 2001;82:267–279.
18. Green WH, Barton PI, Bhattacharjee B, Matheu DM, Schwer DA, Song J, Sumathi R, Carstensen HH, Dean AM, Grenda JM. Computer construction of detailed chemical kinetic models for gas-phase reactors. *Ind Eng Chem Res*. 2001;40:5362–5370.
19. Dente M, Bozzano G, Faravelli T, Marongiu A, Pierucci S, Ranzi E. Kinetic modeling of pyrolysis processes in gas and condensed phase. *Adv Chem Eng*. 2007;32:52.
20. Pierucci S, Ranzi E. A review of features in current automatic generation software for hydrocarbon oxidation mechanisms. *Comput Chem Eng*. 2008;32:805–826.
21. Broadbelt LJ, Stark SM, Klein MT. Termination of computer-generated reaction-mechanisms: species rank-based convergence criterion. *Ind Eng Chem Res*. 1995;34:2566–2573.
22. Truong TN. Reaction class transition state theory: hydrogen abstraction reactions by hydrogen atoms as test cases. *J Chem Phys*. 2000; 113:4957–4964.
23. Sumathi R, Carstensen HH, Green WH. Reaction rate prediction via group additivity Part 1: H abstraction from alkanes by H and CH3. *J Phys Chem A*. 2001;105:6910–6925.
24. Sumathi R, Carstensen HH, Green WH. Reaction rate prediction via group additivity, part 2: H-abstraction from alkenes, alkynes, alcohols, aldehydes, and acids by H atoms. *J Phys Chem A*. 2001; 105:8969–8984.
25. Sumathi R, Carstensen HH, Green WH. Reaction rate predictions via group additivity. Part 3: Effect of substituents with CH2 as the mediator. *J Phys Chem A*. 2002;106:5474–5489.
26. Zhang SW, Truong TN. Kinetics of hydrogen abstraction reaction class H+H-C(sp(3)): first-principles predictions using the reaction class transition state theory. *J Phys Chem A*. 2003;107: 1138–1147.
27. Saeys M, Reyniers MF, Marin GB, Van Speybroeck V, Waroquier M. Ab initio group contribution method for activation energies for radical additions. *AIChE J*. 2004;50:426–444.
28. Sabbe MK, Reyniers MF, Van Speybroeck V, Waroquier M, Marin GB. Carbon-centered radical addition and beta-scission reactions: modeling of activation energies and pre-exponential factors. *ChemPhysChem*. 2008;9:124–140.
29. Sabbe MK, Reyniers MF, Waroquier M, Marin GB. Hydrogen radical addition to unsaturated hydrocarbons and reverse beta-scission reactions: modeling of activation energies and pre-exponential factors. *ChemPhysChem*. 2010;11:195–210.
30. Sabbe MK, Saeys M, Reyniers MF, Marin GB, Van Speybroeck V, Waroquier M. Group additive values for the gas phase standard enthalpy of formation of hydrocarbons and hydrocarbon radicals. *J Phys Chem A*. 2005;109:7466–7480.
31. Sabbe MK, De Vleeschouwer F, Reyniers MF, Waroquier M, Marin GB. First principles based group additive values for the gas phase standard entropy and heat capacity of hydrocarbons and hydrocarbon radicals. *J Phys Chem A*. 2008;112:12235–12251.
32. Sabbe MK, Vandeputte AG, Reyniers MF, Waroquier M, Marin GB. Modeling the influence of resonance stabilization on the kinetics of hydrogen abstractions. *Phys Chem Chem Phys*. 2010;12:1278–1298.
33. Saeys M, Reyniers MF, Van Speybroeck V, Waroquier M, Marin GB. Ab initio group contribution method for activation energies of hydrogen abstraction reactions. *ChemPhysChem*. 2006;7:188–199.
34. Montgomery JA, Frisch MJ, Ochterski JW, Petersson GA. A complete basis set model chemistry. VI. Use of density functional geometries and frequencies. *J Chem Phys*. 1999;110:2822–2827.

35. Montgomery JA, Frisch MJ, Ochterski JW, Petersson GA. A complete basis set model chemistry. VII. Use of the minimum population localization method. *J Chem Phys*. 2000;112:6532–6542.
36. Saeys M, Reyniers MF, Marin GB, Van Speybroeck V, Waroquier M. Ab initio calculations for hydrocarbons: enthalpy of formation, transition state geometry, and activation energy for radical reactions. *J Phys Chem A*. 2003;107:9147–9159.
37. Gomez-Balderas R, Coote ML, Henry DJ, Radom L. Reliable theoretical procedures for calculating the rate of methyl radical addition to carbon-carbon double and triple bonds. *J Phys Chem A*. 2004;108:2874–2883.
38. Sabbe MK, Vandeputte AG, Reyniers MF, Van Speybroeck V, Waroquier M, Marin GB. Ab initio thermochemistry and kinetics for carbon-centered radical addition and beta scission reactions. *J Phys Chem A*. 2007;111:8416–8428.
39. Vandeputte AG, Sabbe MK, Reyniers MF, Van Speybroeck V, Waroquier M, Marin GB. Theoretical study of the thermodynamics and kinetics of hydrogen abstractions from hydrocarbons. *J Phys Chem A*. 2007;111:11771–11786.
40. Bond D. Computational methods in organic thermochemistry. 1. Hydrocarbon enthalpies and free energies of formation. *J Org Chem*. 2007;72:5555–5566.
41. Sundaram KM, Froment GF. Modeling of thermal-cracking kinetics. 3. Radical mechanisms for pyrolysis of simple paraffins, olefins, and their mixtures. *Ind Eng Chem Fund*. 1978;17:174–182.
42. Willems PA, Froment GF. Kinetic modeling of the thermal-cracking of hydrocarbons. 1. Calculation of frequency factors. *Ind Eng Chem Res*. 1988;27:1959–1966.
43. Willems PA, Froment GF. Kinetic modeling of the thermal-cracking of hydrocarbons. 2. Calculation of activation-energies. *Ind Eng Chem Res*. 1988;27:1966–1971.
44. Van Geem KM, Heynderickx GJ, Marin GB. Effect of radial temperature profiles on yields in steam cracking. *AIChE J*. 2004;50:173–183.
45. Van Geem K, Reyniers MF, Marin GB. Challenges of modeling steam cracking of heavy feedstocks. *Oil Gas Sci Technol Revue de l'institut français du pétrole*. 2008;63:79–94.
46. Barendregt S, Dente M, Ranzi E. Calculations concerning the production of ethylene by thermal cracking. *Polytechnisch Tijdschrift Procestechniek/Polytechnisch Tijdschrift Procestechniek*. 1981;11:573–579.
47. van Goethem MWM, Barendregt S, Grievink J, Moulijn JA, Verheijen PJT. Ideal chemical conversion concept for the industrial production of ethene from hydrocarbons. *Ind Eng Chem Res*. 2007;46:4045–4062.
48. Chevalier C, Warnatz J, Melenk H. Automatic generation of reaction-mechanism for the oxidation of higher hydrocarbons. *Berichte Der Bunsen-Gesellschaft Phys Chem Chem Phys*. 1990; 94.
49. Quann RJ, Jaffe SB. Structure-oriented lumping: describing the chemistry of complex hydrocarbon mixtures. *Ind Eng Chem Res*. 1992;31:2483–2497.
50. Broadbelt LJ, Stark SM, Klein MT. Computer-generated pyrolysis modeling: on-the-fly generation of species, reactions, and rates. *Ind Eng Chem Res*. 1994;33:790–799.
51. Blurock ES. Reaction—system for modeling chemical reactions. *J Chem Inf Comput Sci*. 1995;35.
52. Ranzi E, Faravelli T, Gaffuri P, Sogaro A. Low temperature combustion—automatic-generation of oxidation reactions and lumping procedures. *Combust Flame*. 1995;102.
53. Susnow RG, Dean AM, Green WH, Peczak P, Broadbelt LJ. Rate-based construction of kinetic models for complex systems. *J Phys Chem A*. 1997;101:3731–3740.
54. Prickett SE, Mavrovouniotis ML. Construction of complex reaction systems. 1. Reaction description language. *Comput Chem Eng*. 1997;21:1219–1235.
55. Warth V, Battin-Leclerc F, Fournet R, Glaude PA, Côme GM, Scacchi G. Computer based generation of reaction mechanisms for gas-phase oxidation. *Comput Chem*. 2000;24:541–560.
56. Klein MT, Hou G, Bertolacini RJ, Broadbelt LJ, Kumar A. *Molecular Modeling in Heavy Hydrocarbon Conversions*. Boca Raton: Taylor & Francis Group, 2006.
57. Rice FO. The thermal decomposition of organic compounds from the standpoint of free radicals I. Saturated hydrocarbons. *J Am Chem Soc*. 1931;53:1959–7219.
58. Rice FO. The thermal decomposition of organic compounds from the standpoint of free radicals III. The calculation of the products formed from paraffin hydrocarbons. *J Am Chem Soc*. 1933;55:3035–3040.
59. Kossiakoff A, Rice FO. Thermal decomposition of hydrocarbons, resonance stabilisation and isomerization of free radicals. *J Am Chem Soc*. 1943;65:590.
60. Laidler KJ. *Chemical Kinetics*. New York: Harper & Row, 1987.
61. Li S, Petzold LR. Design of New DASPK for Sensitivity Analysis. *UCSB Technical Report*. 1999.
62. Klippenstein SJ, Georgievskii Y, Harding LB. Predictive theory for the combination kinetics of two alkyl radicals. *Phys Chem Chem Phys*. 2006;8:1133–1147.
63. Georgievskii Y, Klippenstein SJ. Variable reaction coordinate transition state theory: analytic results and application to the C2H3+H -> C2H4 reaction. *J Chem Phys*. 2003;118:5442–5455.
64. Harding LB, Georgievskii Y, Klippenstein SJ. Predictive theory for hydrogen atom: hydrocarbon radical association kinetics. *J Phys Chem A*. 2005;109:4646–4656.
65. Harding LB, Klippenstein SJ, Georgievskii Y. On the combination reactions of hydrogen atoms with resonance-stabilized hydrocarbon radicals. *J Phys Chem A*. 2007;111:3789–3801.
66. CHEMKIN Release 4.1.1 [computer program]. San Diego, CA: Reaction Design, Inc., 2007.
67. Hottel HC, Sarofim AF. *Radiative Transfer*. New York: McGraw-Hill, 1967.
68. Vercammen HAJ, Froment GF. An improved zone method using Monte-Carlo techniques for the simulation of radiation in industrial furnaces. *Int J Heat Mass Transfer*. 1980;23:329–337.
69. Rao MVR, Plehiers PM, Froment GF. The coupled simulation of heat-transfer and reaction in a pyrolysis furnace. *Chem Eng Sci*. 1988;43:1223–1229.
70. Plehiers PM, Froment GF. Firebox simulation of olefin units. *Chem Eng Commun*. 1989;80:81–99.
71. Broadbelt LJ, Stark SM, Klein MT. Termination of computer-generated reaction-mechanisms: species rank-based convergence criterion. *Ind Eng Chem Res*. 1995;34:2566–2573.
72. Song J. *Building Robust Chemical Reaction Mechanisms: Next Generation of Automatic Model Construction Software PhD dissertation*. Massachusetts Institute of Technology, Cambridge, MA; 2004.
73. Wauters S, Marin GB. Kinetic modeling of coke formation during steam cracking. *Ind Eng Chem Res*. 2002;41:2379–2391.
74. Reyniers MFSG, Froment GF. Influence of metal-surface and sulfur addition on coke deposition in the thermal-cracking of hydrocarbons. *Ind Eng Chem Res*. 1995;34:773–785.
75. Dhuyvetter I, Reyniers MF, Froment GF, Marin GB, Viennet D. The influence of dimethyl disulfide on naphtha steam cracking. *Ind Eng Chem Res*. 2001;40:4353–4362.
76. Curran HJ. Rate constant estimation for C-1 to C-4 alkyl and alkoxyl radical decomposition. *Int J Chem Kinet*. 2006;38:250–275.
77. Miller JA, Klippenstein SJ. The H+C2H2 (+M) reversible arrow C2H3 (+M) and H+C2H2 (+M) reversible arrow C2H5 (+M) reactions: electronic structure, variational transition-state theory, and solutions to a two-dimensional master equation. *Phys Chem Chem Phys*. 2004;6:1192–1202.
78. Matheu DM, Grenda JM. A systematically generated, pressure-dependent mechanism for high-conversion ethane pyrolysis. 1. Pathways to the minor products. *J Phys Chem A*. 2005;109:5332–5342.
79. Miller JA, Klippenstein SJ. The recombination of propargyl radicals and other reactions on a C6H6 potential. *J Phys Chem A*. 2003;107:7783–7799.
80. Lindstedt RP, Rizos KA. The formation and oxidation of aromatics in cyclopentene and methyl-cyclopentadiene mixtures. *Proc Combust Inst*. 2002;29:2291–2298.
81. Gueniche HA, Glaude PA, Fournet R, Battin-Leclerc F. Rich methane premixed laminar flames doped by light unsaturated hydrocarbons—III. Cyclopentene. *Combust Flame*. 2008;152:245–261.
82. Bird RB, Lightfoot WE. *Transport Phenomena*. New York: J. Wiley, 2001.

Manuscript received Nov. 5, 2009, and revision received Mar. 25, 2010.